IOPscience iopscience.iop.org

Home Search Collections Journals About Contact us My IOPscience

Land cover and land use changes in the oil and gas regions of Northwestern Siberia under changing climatic conditions

This content has been downloaded from IOPscience. Please scroll down to see the full text.

2015 Environ. Res. Lett. 10 124020

(http://iopscience.iop.org/1748-9326/10/12/124020)

View the table of contents for this issue, or go to the journal homepage for more

Download details:

IP Address: 210.77.64.105
This content was downloaded on 17/04/2017 at 04:47

Please note that terms and conditions apply.

You may also be interested in:

Regional and landscape-scale variability of Landsat-observed vegetation dynamics in northwest Siberian tundra
Gerald V Frost, Howard E Epstein and Donald A Walker

Spatial heterogeneity of greening and browning between and within bioclimatic zones in northern West Siberia
Victoria V Miles and Igor Esau

Spatial and temporal patterns of greenness on the Yamal Peninsula, Russia: interactions ofecological and social factors affecting the Arctic normalized difference vegetationindex
D A Walker, M O Leibman, H E Epstein et al.

Drivers of tall shrub proliferation adjacent to the Dempster Highway, Northwest Territories, Canada
Emily A Cameron and Trevor C Lantz

Increased wetness confounds Landsat-derived NDVI trends in the central Alaska North Slope region, 1985–2011
Martha K Raynolds and Donald A Walker

The response of Arctic vegetation to the summer climate: the relation between shrub cover,NDVI, surface albedo and temperature
Daan Blok, Gabriela Schaepman-Strub, Harm Bartholomeus et al.

Spatial variation in vegetation productivity trends, fire disturbance, and soil carbon across arctic-boreal permafrost ecosystems
Michael M Loranty, Wil Lieberman-Cribbin, Logan T Berner et al.

Environmental Research Letters

LETTER

Land cover and land use changes in the oil and gas regions of Northwestern Siberia under changing climatic conditions

Qin Yu[1,6], **Howard E Epstein**[2], **Ryan Engstrom**[1], **Nikolay Shiklomanov**[1,3] **and Dmitry Strelestskiy**[1,4,5]

[1] Department of Geography, the George Washington University, USA
[2] Department of Environmental Sciences, University of Virginia, USA
[3] Tyumen State Oil and Gas University, Tyumen, Tyumen Oblast 625000, Russia
[4] State Hydrological Institute, St. Petersburg, Russia
[5] Earth Cryosphere Institute, SB RAS Tyumen, Russia
[6] Author to whom any correspondence should be addressed.

E-mail: qinyu@gwu.edu

Keywords: arctic ecosystems, Corona, land use change, Quickbird, permafrost, remote sensing indices, Landsat

OPEN ACCESS

RECEIVED
14 July 2015

REVISED
23 November 2015

ACCEPTED FOR PUBLICATION
25 November 2015

PUBLISHED
17 December 2015

Content from this work may be used under the terms of the Creative Commons Attribution 3.0 licence.

Any further distribution of this work must maintain attribution to the author(s) and the title of the work, journal citation and DOI.

Abstract

Northwestern Siberia has been undergoing a range of land cover and land use changes associated with climate change, animal husbandry and development of mineral resources, particularly oil and gas. The changes caused by climate and oil/gas development Southeast of the city of Nadym were investigated using multi-temporal and multi-spatial remotely sensed images. Comparison between high spatial resolution imagery acquired in 1968 and 2006 indicates that 8.9% of the study area experienced an increase in vegetation cover (e.g. establishment of new saplings, extent of vegetated cover) in response to climate warming while 10.8% of the area showed a decrease in vegetation cover due to oil and gas development and logging activities. Waterlogging along linear structures and vehicle tracks was found near the oil and gas development site, while in natural landscapes the drying of thermokarst lakes is evident due to warming caused permafrost degradation. A Landsat time series dataset was used to document the spatial and temporal dynamics of these ecosystems in response to climate change and disturbances. The impacts of land use on surface vegetation, radiative, and hydrological properties were evaluated using Landsat image-derived biophysical indices. The spatial and temporal analyses suggest that the direct impacts associated with infrastructure development were mostly within 100 m distance from the disturbance source. While these impacts are rather localized they persist for decades despite partial recovery of vegetation after the initial disturbance and can have significant implications for changes in permafrost dynamics and surface energy budgets at landscape and regional scales.

1. Introduction

Changes in climate, vegetation, and human activities can have profound impacts on arctic ecosystems (Bhatt *et al* 2010, Walker *et al* 2011). These ecosystems are unique, fragile, and sensitive to climate change (Perovich *et al* 2013) and other anthropogenic impacts (e.g. Kumpula *et al* 2011). Changes caused by accelerated climate warming in the Arctic are found to be more substantial and happening at faster rates when compared with many other parts of the world (Turner *et al* 2003, ACIA 2005, Ford *et al* 2006). Such changes include sea ice decline (Stroeve *et al* 2012), permafrost degradation (Streletskiy *et al* 2014), and shrub expansion (Frost *et al* 2013). Additionally, exploration and development of vast hydrocarbon deposits have intensified in many regions of the Arctic (Kumpula *et al* 2011). Subsequent impacts of associated human activities on arctic ecosystems affect local vegetation, hydrological and surface reflectivity properties directly and can also cause changes to the underlying permafrost conditions. However, much of current research has only focused on changes associated either with climate or land use at local scales (but see Raynolds *et al* 2014). The extent and temporal dynamics of changes due to climate and industrial development and how these changes evolve at landscape and regional scales is currently understudied but crucial

© 2015 IOP Publishing Ltd

for assessing and projecting arctic ecosystem dynamics in the future.

The dynamic interactions among different components of the arctic system result in a complex response and interaction of the arctic environment to climate-induced changes. For example, sea ice decline reduces albedo (a measure of percent energy/radiation being reflected) and may contribute to the summer warming of arctic coastal areas and an increase in vegetation productivity (Chapin *et al* 2005, Bhatt *et al* 2010, 2013, Epstein *et al* 2012). Analyses of the Advanced Very High Resolution Radiometer (AVHRR)-derived Normalized Difference Vegetation Index (NDVI) reveal a 'greening' trend in arctic tundra vegetation which is consistent with the increase in near-surface air temperatures throughout the Arctic (Jia *et al* 2003, Goetz *et al* 2005, Bhatt *et al* 2010, 2013). Although these analyses reveal broad-scale trends, substantial variation in vegetation responses to climate occur at finer spatial scales (Moskalenko 2012a, 2012b). Significant tall shrub expansion over the last five decades was reported at several undisturbed sites in West Siberia and attributed to strong regional climatic warming (Frost *et al* 2013). Yet the direct and indirect effects of shrub expansion on energy balance and permafrost stability remain unclear since shrub may provide shade and protection to permafrost in summer but traps more snow in winter that leads to soil warming than other type of tundra such as sedge-graminoid tundra (Blok *et al* 2010).

The assessment of long-term vegetation change at the regional scale is complicated by distinguishable anthropogenic pressures exerted on the fragile arctic environment (Forbes *et al* 2001, 2009, Kumpula *et al* 2010, 2011, Walker *et al* 2011). Development of human infrastructure is almost always associated with disturbance that removes natural vegetation cover, alters surface and subsurface hydrology and the ground thermal regime, and changes soil structure and biogeochemistry (Auerbach *et al* 1997,Raynolds *et al* 2014, Streletskiy *et al* 2014). As such, human-induced land cover and land use changes can exacerbate impacts of climate change, causing potentially detrimental consequences for arctic ecosystems (Pielke 2002, Hinzman *et al* 2005, Huntington *et al* 2007, Larsen *et al* 2014).

Intense anthropogenic pressures have already affected large tracts of the Arctic (Larsen and Fondahl 2015). Relatively small clusters of economic activity and infrastructure in North America, mainly on the North Slope of Alaska, are dwarfed by industrial development that has occurred in some regions of the Russian Arctic after the discovery of hydrocarbon deposits in the 1950s (Armstrong *et al* 1978, Flanders *et al* 1998). In particular in Northwest Siberia over 200 million hectares of swamp area has become a 'hot spot' of human activity (Armstrong *et al* 1978, Khitun *et al* 2001, Walker *et al* 2011, Kumpula *et al* 2011). Over the last forty years major engineering works, such as oil and gas production fields, transportation corridors, pipelines, power plants, mining infrastructure and cities, have been developed within the region. An extensive network of vehicle tracks and rudimentary trails traverses the areas outside of engineering facilities since none of the oil and gas fields are near potential users, and transportation is the key to the economic development (Armstrong *et al* 1978). Such anthropogenic pressure has caused extensive land degradation in some regions (Forbes *et al* 2001, 2006, Kumpula *et al* 2012). In particular, extensive disturbance of vegetation cover has altered the surface radiation balance and surface/subsurface hydrology, promoting changes in the ground thermal regime, and causing degradation of permafrost (e.g. Moskalenko 2003, Vasiliev *et al* 2008a, 2008b). Simultaneously, the West Siberian region has experienced a rapid rate of air temperature and precipitation increase (ACIA 2005, Streletskiy *et al* 2012, Larsen *et al* 2014), resulting in complex interplay between human- and climate-induced impacts on the land surface (Moskalenko 2012a, 2012b, Larsen and Fondahl 2015).

Studies of the anthropogenic effects on arctic ecosystems have been limited to short-to mid-term field studies and aerial surveys at areas immediately at or adjacent to the disturbance (e.g. Walker *et al* 1987, Walker and Walker 1991, Moskalenko *et al* 1998 but see Raynolds *et al* 2014). Although those studies provided valuable insights into human-induced impacts on ecosystems, it would be costly to assess such changes and impacts repeatedly on the ground. Satellite-based remote sensing has been widely used to detect land cover and land use dynamics (e.g. Turner *et al* 1995) and can complement field studies by observing ecosystem change at a range of spatial scales and potentially over relatively long time periods. Walker *et al* (2009) used a relatively long (25 year) time series of coarse-resolution (AVHRR) satellite imagery for the Yamal Peninsula, Russia to evaluate the spatial/temporal dynamics of development and land use change. However, identifying the detailed relations between the vegetation properties and human disturbance at more localized spatial scales requires high spatial resolution satellite imagery (tens of meters or finer). Recent research by Raynolds *et al* (2014) assessed aerial photographs collected during 1949–2011 in the Prudhoe Bay Oilfield, Alaska, and demonstrated the progression of thermokarst as a result of impacts from infrastructure and climate change in ice-rich permafrost landscapes. While this is an important case study it is difficult to expand this research methodology to the heterogeneous and relatively data limited areas that dominate the vast majority of the Arctic.

In this study, we assess the ecosystem changes in response to climate change and oil/gas development related to land use in West Siberia through the lens of satellite imagery of a range of spatial and temporal

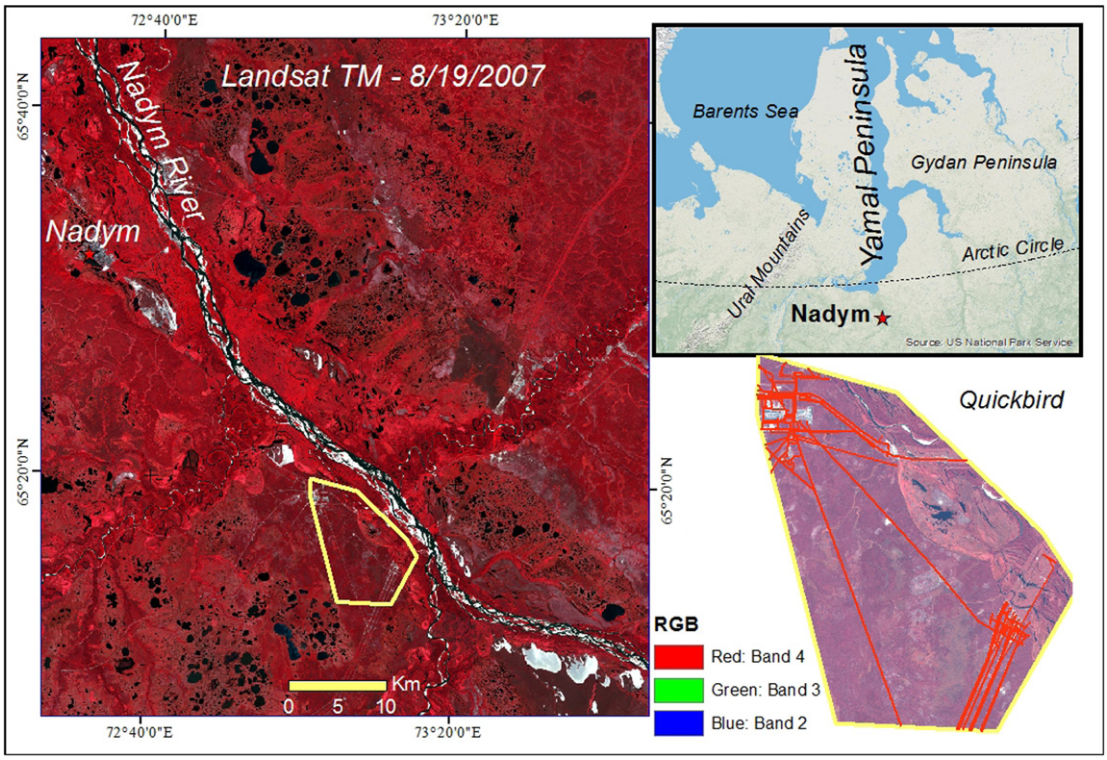

Figure 1. Study region shown in a Landsat TM scene (2007) of approximately 5625 km^2. The yellow polygon on the Landsat scene outlines the extent of a Quickbird image, shown in lower right. The images are shown with the band combinations: red-NIR band, green–red band, blue–green band.

scales. The research methodology described in this study can be readily applied to many regions of the Arctic where medium resolution dataset such as Landsat are available. Our research goals are threefold: (1) to determine satellite datasets that are useful to document changes over the past four decades; (2) to assess land cover and land use changes in a forest-tundra region associated with climate change, and oil and gas development and related human activities; (3) to assess the spatial and temporal impacts of development utilizing remote sensing derived surface properties.

2. Materials and methods

2.1. Study region

The study region encompasses the city of Nadym, Russia at 65°32' N and 72°31'E (figure 1), which is located to the South of the Yamal Peninsula, in Northwestern Siberia. Nadym is currently one of the largest cities in Northwestern Siberia with a population of about 50 000. It became the main gas center of the Nadym-Pur region since the discovery of commercial quantities of gas deposits in 1966, and experienced a population increase as exploration and development started gradually in the early 1970s (Armstrong *et al* 1978). The mean annual air temperature is −5.9 °C, and the mean summer air temperature is 10.8 °C, with mean annual temperature increasing more than 2 °C since the late 1960s (Vikhamar-Schuler *et al* 2010, Streletskiy *et al* 2012). The growing season normally extends from late May to mid-October. This region lies within the discontinuous permafrost zone, with permafrost mostly confined to peatlands and frost-heaved mounds (Vasilev 2008). Since 1970 permafrost temperatures at a depth of 10 m (layer with minimum annual fluctuations of temperatures) have increased from −1.8 °C to −0.4 °C, and the active layer depth has increased by 30% (Moskalenko 2012b). Two field sites at Nadym were sampled for zonal vegetation analyses in 2007, close to a site of the Circumpolar Active Layer Monitoring project (Walker *et al* 2008). Well-drained locations along the river valleys are covered by boreal forest with tundra vegetation present. The trees are mainly Scots pine (*Pinus sylvestris*) and mountain birch (*Betula tortuosa*) mixed with Siberian larch (*Larix sibirica*). The understory consists of dwarf shrubs (*Ledum palustre*, *Betula nana*, *Empetrum nigrum*, *Vaccinium uliginosum*, *V. vitis-idaea*), lichens (mainly *Cladonia stellaris*) and mosses (mainly *Pleurozium schreberi*). In areas affected by frost heave, sparse cedar (*Pinus sibirica*) forests with wild rosemary-lichen communities and wild rosemary-*Sphagnum*-lichen communities predominate (Walker *et al* 2008).

2.2. Data sources

A suite of multi-temporal and multi-sensor remotely sensed imagery, including high resolution Corona

photos (available from 1959 to 1972), Quickbird-2 imagery (since 2001) and Landsat images (since 1972), were collected for this study. The selected images were acquired during the growing season, preferably during the peak of the growing season, which generally ranges from mid-July to early-September in high latitude regions (Jia *et al* 2009). Our high spatial resolution imagery includes three Corona images acquired on 21 August 1968 and a Quickbird-2 image acquired on 6th September, 2006. The Corona images are declassified, Cold War era satellite surveillance system images taken across the study region (and other regions in Russia and elsewhere) from 1963 to 1980, which are panchromatic photography with large swath widths and varying ground resolutions (0.6–150 m). Our more recent dataset was from the Very High Resolution (VHR) commercial earth observation sensor Quickbird-2 (available since 2001). It collects imagery with 0.61 m panchromatic and 2.4 m multispectral resolution in the blue (0.430–0.545 μm), green (0.466–0.620 μm), red (0.590–0.710 μm) and near infrared (NIR, 0.715–0.918 μm) wavelengths. When paired with Corona satellite photography as a baseline dataset, Quickbird data can document land-cover changes over the past forty years with very high spatial resolution. Landsat image series data provide the longest record (1972—present) of moderate resolution (30–79 m spatial resolution) multispectral data available. Multi Spectral Scanner (MSS) on board Landsat 1 collected images in four spectral bands (Band 4—green (0.5–0.6 μm), Band 5—red (0.6–0.7 μm), Band 6—near IR (0.7–0.8 μm) and Band 7—near IR (0.8–1.1 μm)) with a spatial resolution of 79 m. Landsat Thematic Mapper (TM) imagery consists of seven spectral bands (blue (0.45–0.52 μm), green (0.52–0.60 μm), red (0.63–0.69 μm), NIR (0.76–0.90 μm), Mid-IR (1.55–1.75 μm and 2.08–2.35 μm) and thermal IR (10.40–12.5 μm)) with a spatial resolution of 30 m for Bands 1–5 and 7 (http://landsat.usgs.gov/band_designations_landsat_satellites.php). The spectral information can be used to derive indices that are related to environmental variables such as vegetation greenness, surface moisture and surface material reflectivity. When available, Landsat TM Climate Data Records (CDR) Dataset images were used in this study due to their sophisticated atmospheric corrections (Masek *et al* 2006). The CDR are high level Surface Reflectance Data products that support land surface change studies. The dataset is generated from the Landsat Ecosystem Disturbance Adaptive Processing System (LEDAPS), which applies Moderate Resolution Imaging Spectroradiometer (MODIS) atmospheric correction routines to Level-1 Landsat data products. Effects from clouds, water vapor, ozone, and aerosol optical thickness are minimized through LEDAPS (Masek *et al* 2006). Table 1 lists the basic spectral, spatial, and temporal information of the images.

Table 1. Imagery collected for use in this study included a pair of VHR imagery of less than 2.4 m of spatial resolution for visual change detection. Landsat images from MSS and TM sensors (79 m and 30 m spatial resolution, respectively) were acquired for quantitative spatial and temporal analysis.

Mission and sensor	Date	Spectral bands	Pixel resolution
Corona	8/21/1968	Pan	2 m
Quickbird	9/6/2006	Multi	2.4 m
		Pan	0.6 m
Landsat-1, MSS	6/17/1973	Multi	79 m
Landsat-4, TM	6/19/1988	Multi	30 m
Landsat-5, TM	9/13/1987, 6/30/1989, 8/17/1989, 6/17/1990, 7/19/1990, 7/15/2006, 7/18/2007, 8/19/2007, 7/23/2009, 5/26/2011, 6/27/2011, 9/15/2011	Multi	30 m

2.3. Imagery processing and biophysical index derivation

The Corona images were geo-referenced, mosaicked, and co-registered with the Quickbird imagery to allow for change detection. Landsat images from 1973 to 2011 were collected from the USGS Earth Resources Observation and Science Center Science Processing Architecture On Demand Interface (https://espa.cr.usgs.gov/). The datasets, except the MSS scene, were pre-processed using LEDAPS. To minimize the impact from cloud cover, only images with less than 20% cloud cover were selected for this study. All images were geo-referenced to each other, and subsets were extracted for an area covering the Nadym city and the old oil/gas facility. Biophysical indices, including NDVI (Rouse *et al* 1974), albedo (Liang 2001), and Normalized Difference Water Index (NDWI) (Gao 1996) were calculated from surface reflectances collected by the Landsat series for each scene, except that only NDVI was calculated for the MSS scene.

NDVI is a widely used index for assessing vegetation condition, as it is a proxy for photosynthetic activity of green vegetation. Although it is not an intrinsic physical quantity, it does correlate with certain physical properties of the vegetation canopy such as the amount of leaf area, fractional vegetation cover, vegetation condition and biomass (Carlson and Ripley 1997). NDVI was calculated with the following equation:

$$\mathrm{NDVI} = (\rho_{\mathrm{NIR}} - \rho_{\mathrm{RED}})/\left(\rho_{\mathrm{NIR}} + \rho_{\mathrm{RED}}\right) \text{or NDVI} = (\rho_4 - \rho_3)/\left(\rho_4 + \rho_3\right),$$

where ρ_{RED} and ρ_{NIR} stand for the spectral reflectivity acquired in the red and near-infrared wavelength intervals, i.e. band 3 (0.63–0.69 μm) and band 4 (0.76–0.90 μm) of Landsat TM images and band 5

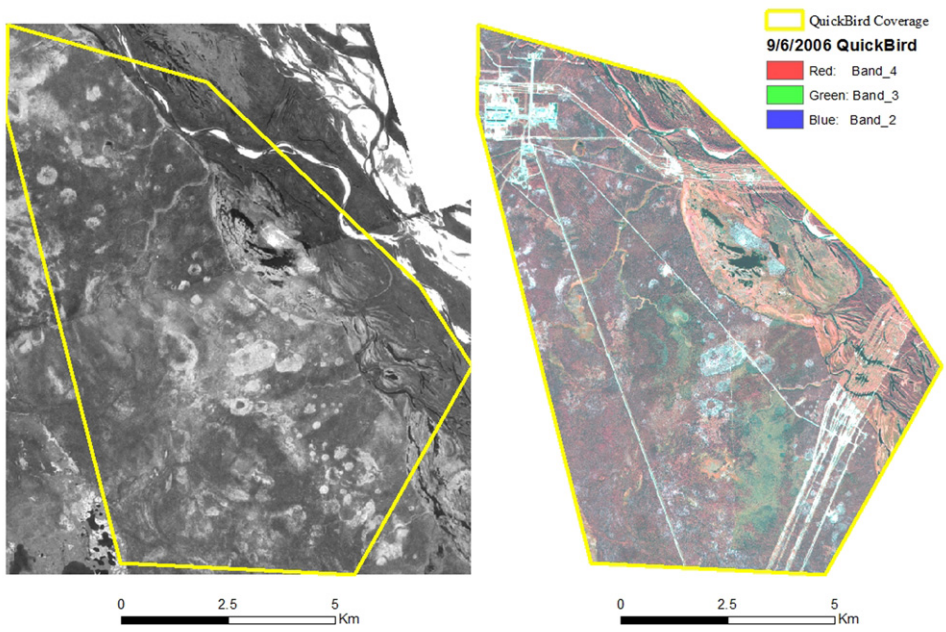

Figure 2. Co-registered Corona imagery (left) and Quickbird imagery (right). The yellow outlines the visual change analysis region (the Quickbird scene is ~90 km^2 and does not cover the Nadym city). The 1968 Corona image was taken before the extensive development of the Medvejie gas field and shows a flat, poorly drained watershed of the Nadym River dotted by numerous thermokarst lakes at the forest-tundra ecotone. The 2006 Quickbird image shows areas of development, such as a settlement around the pump station in the upper left corner, numerous linear features such as two power lines and a gas pipeline radiating Southeast, a series of roads going East from the pump station, and a network of roads in the lower right corner.

(0.6–0.7 μm) and band 7 (0.8–1.1 μm) for Landsat MSS images. The normalization cancels out a large proportion of noise caused by changing sun angles, topography, shadow, clouds and other atmospheric conditions. NDVI ranges between −1 and +1.

Albedo indicates the degree to which a surface reflects solar energy and is a non-dimensional, unitless quantity, varying between 0 and 1. It is a critical variable affecting surface energy budget and the Earth's climate. Melting of sea ice has contributed to the acceleration of Arctic warming, since high albedo sea ice is replaced with low albedo water, causing more energy to be absorbed by water rather than being reflected. Since land use change alters land cover through associated human activities, it will likely affect the surface energy budget. Land surface broadband albedo was estimated using the equation derived by Liang (2001) for Landsat ETM+. We assumed the surface was Lambertian, and used reflectance of each band to calculate broadband albedo as follows:

$$\text{Albedo} = 0.356\rho_1 + 0.130\rho_3 + 0.373\rho_4 + 0.085\rho_5 + 0.072\rho_7 - 0.0018,$$

where $\rho_{1,3,4,5,7}$ are the narrow band reflectances.

NDWI, a more recently developed index calculated from the NIR and shortwave infrared channels, captures changes in both surface water content and water in vegetation canopies (Gao 1996). NDWI ranges between −1 and +1. Negative values in NDWI are generally associated with dry bare soils

$$\text{NDWI} = (\rho_{0.86\,\mu\text{m}} - \rho_{1.24\,\mu\text{m}})/\left(\rho_{0.86\,\mu\text{m}} + \rho_{1.24\,\mu\text{m}}\right)$$
$$\text{or NDWI} = (\rho_4 - \rho_5)/\left(\rho_4 + \rho_5\right),$$

where $\rho_{0.86\,\mu\text{m}}$ and $\rho_{1.24\,\mu\text{m}}$ are apparent reflectances at 0.86 and 1.24 μm wavelengths. For Landsat TM specifically, these are band 4 (0.76–0.90 μm) and band 5 (1.55–1.75 μm).

2.4. Change analysis

We first quantified the changes in land cover based on high spatial resolution image pair. The Corona scene is a panchromatic image and not suitable for spectral quantitative classification, however due to its high spatial resolution (2 m) which is comparable to the Quickbird image (panchromatic band of 0.6 m and multispectral bands of 2.4 m), it can provide a baseline from which changes in land cover and land use can be evaluated (figure 2). Utilizing the image pair we can visually identify tall shrubs and boreal trees through their structural differences relative to tundra vegetation, and water bodies through their distinct spectral and spatial characteristics (Grosse *et al* 2005). To quantify changes caused by either climate change or land use, we digitized areas with substantial changes with respect to vegetation density and extent, water bodies and land use in areas with minimal human development activities and areas with substantial land use such as roads, facilities, pipelines and logging.

Second, to assess long term changes due to land use, linear features (pipelines, permanent roads and vehicle tracks) and industrial facilities were digitized utilizing the 2006 Quickbird imagery as the reference data source since none of the changes had been initiated at the time of the Corona scene. Then, a series of buffer zones were generated along the digitized linear structures and production facilities at 30 m intervals up to 600 m away from the oil/gas industrial facility. Mean values of Landsat MSS-derived NDVI and Landsat TM-derived NDVI, albedo and NDWI were calculated as a function of distance from disturbance. Disturbance in this study is considered to be infrastructure or other anthropogenic land cover change that alters vegetation, surface moisture and land cover type with respect to surface albedo. We used the 2006 high-resolution Quickbird image to digitize the major developments (i.e. disturbances), and created buffer zones using those as the center. Then zonal statistics were conducted on images from different years. Each image in the analysis was 'zoned' with respect to distance from the 'disturbance center,' and mean NDVI, NDWI and albedo were calculated.

Third, mean NDVI values across the buffer zones were compared between the Landsat-1 MSS acquired on June 19th, 1973 and Landsat-5 TM acquired on June 19th, 1990. These anniversary date images minimize any effect of vegetation phenology on NDVI variability and allow for the spatial patterns to be analyzed. Fourth, in order to understand how NDVI, albedo and NDWI varied across phenological stages and how consistently these data are related to spatial patterns due to disturbance during the growing season (particularly peak growing season), we acquired and analyzed five images in 2007 (15th May, 18th July, 19th August, 4th September and 20th September). Such assessment may benefit other potential studies to select usable imagery where cloud cover may pose problems in deriving usable indices. Finally, we compared the distance from disturbance patterns for scenes from peak growing season (mid-July) in years 1990, 2006, 2007 and 2009 to assess how the spatial patterns associated with disturbances evolve over the most recently available time period, and to determine how vegetation changes over this period.

3. Results

3.1. Land cover change associated with climate warming

Various land cover changes were detected with respect to changes in vegetation extent and density, and hydrological conditions based on the comparison between the two high spatial resolution images (figures 2, 3 and 4). Within the undisturbed areas, areas where climate change is the dominant factor, vegetation cover has increased, largely due to increased tree cover and density (e.g. green outlined area in figures 3(a) and (b)). The estimated area with vegetation increase is about 7.76 km^2 (8.9% of total Quickbird image coverage). Several thermokarst lakes (ranging in size from 10 m to 25 m in diameter) outlined in red (figure 4(a)) have either decreased in size or drained completely (figure 4(b)).

3.2. Land cover change associated with land use

There were no human activity related disturbances found in the 1968 Corona images (figure 1). However, extensive oil and gas related developments are apparent in the Quickbird scene acquired in 2006, such as facility structures, roads, and vehicle tracks. Total vegetated area decreased about 7.98 km^2 (9.1%) including about a 1.49 km^2 (1.7%) decrease due to logging. The comparison of Corona and Quickbird images also reveals changes in hydrological features (figure 4). In the area with disturbance such as roads, a previously drained lake (figure 4(c)) accumulated water and became a lake about 50 m wide after the construction of the road (figure 4(d)).

Multi-temporal Landsat imagery added temporal dynamics to the change analysis solely based on the VHR image pair. Vegetation changes in the study region between 1968 and 2006 were not unidirectional (figure 5). Recovery of vegetation from disturbed areas (e.g., area outlined in black) was documented by Landsat images (2007, figures 5(b) and (d)), as well as by the Quickbird (2006) image. The original vegetated surface was dramatically disturbed between 1968 (figure 5(a)) and 1988 (figure 5(b)). For example, comparing the Landsat scenes acquired in 1988 and 2007, both red and black polygons in figure 5 outline areas with substantial vegetation change. On the 1988 image acquired on 19th June , the red polygon outlines an area possibly affected by a local disturbance event, likely to be a light/crown fire which did not cause severe damage to the trunks. This disturbance assessment is based on the mean NDVI of and NDWI dropping to 0.40 and −0.13, respectively relative to the mean NDVI and NDWI 0.65 and 0.24 extracted from an image acquired in 2007. The area outlined in black in figures 5(b) and (d) demonstrates the impacts of vehicle tracks over time with a mean NDVI and NDWI of −0.1 and −0.10 in 1988 relative to the 0.69 and 0.25 in measured in 2007. Both areas have recovered to a certain extent from disturbance impacts. Although partially recovered, the impacts of vehicle tracks are still evident where the tracks cross lakes and streams (indicated by blue arrows in figure 5).

3.3. Spatial and temporal pattern of land use impacts

The spatial pattern of land use impacts was examined by determining the amount of change in NDVI, albedo and NDWI at multiple distances away from the oil and gas infrastructure. The spatial patterns (1) before and after disturbance; (2) with seasonal variations in 2007

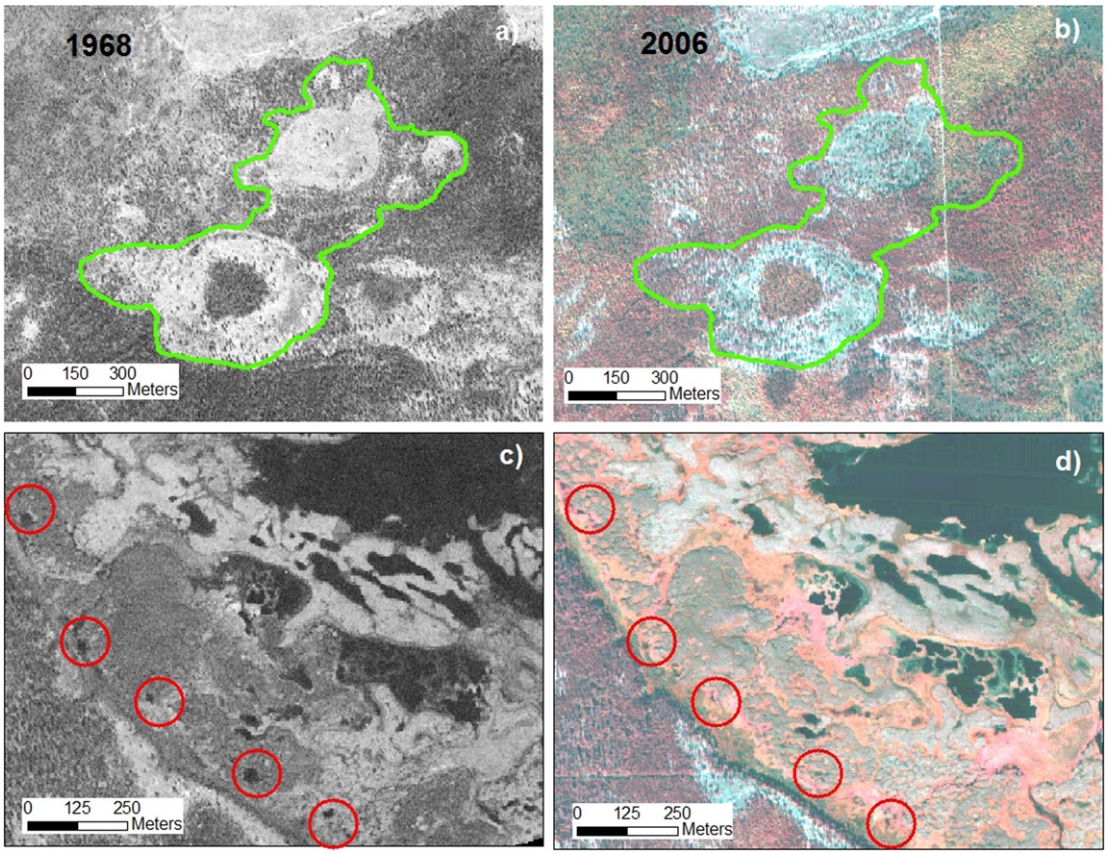

Figure 3. Comparison of land cover between 1968 Corona and 2006 Quickbird images is shown. The upper pair indicates increased tree extent and density (e.g. outlined in green) in undisturbed areas, reflecting positive response of vegetation to climate warming. The lower pair highlights the changes in thermokarst lakes between 1968 (a) and 2006 (b) without much human activity associated disturbance, indicating thawing permafrost that leads to underground drainage.

and (3) during mid-growing season across multiple years are presented.

3.3.1. Spatial pattern comparison before and after disturbance

Mean NDVI values along the disturbed area were compared for the Landsat MSS and TM scenes acquired on 6/17 in 1973 and 1990, respectively. Mean NDVI along the twenty buffered zones (30 m each, 600 m wide) varied little in the Landsat MSS image from 1973 (figure 6). While 1990 showed the impact of the oil and gas associated disturbance with very low NDVI in areas within approximately 100 m of the disturbance and then little variation past this distance (figure 6).

3.3.2. Seasonal variation of spatial pattern due to disturbance in 2007

Seasonal variations in the impacts of disturbance were investigated using Landsat imagery derived metrics (NDVI, albedo, and NDWI) calculated for multiple dates during the 2007 growing season (figure 7). On 5th May, 2007, mean NDVI within the buffer zones (ranging from 30 m to 600 m) remained less than 0.1, indicating limited vegetation growth at this time. Surface albedo was between 0.2 and 0.3, and mean NDWI was >0.6, indicating partial melt in the study region had begun in May 2007. As the growing season progressed, NDVI reached a peak between 18th July and 4th September and then declined on 20th September . Surface albedo decreased slightly ($\sim$0.01) as it progressed later into the growing season, but the variation among dates was significant ($\pm$0.1). The mean albedo within the disturbed buffer zones (30 and 60 m) was consistently 0.04 ($\pm$0.02) higher than in less disturbed buffer zones ($>$90 m from the disturbance). During the growing season, the mean NDWI within the 30 and 60 m buffer zones (near the disturbance) was consistently 0.20 ($\pm$0.02) lower than in buffer zones further away, indicating less moisture at the surface of more disturbed zones compared to the less disturbed zones that are farther away from disturbance.

In general, all three calculated indices (NDVI, albedo and NDWI) show that substantial changes occurred within a 100 m distance from the disturbance, and there was not a substantial difference beyond that range. Averages of NDVI, albedo and NDWI are consistent across all study years, but show some variations due to growing season differences.

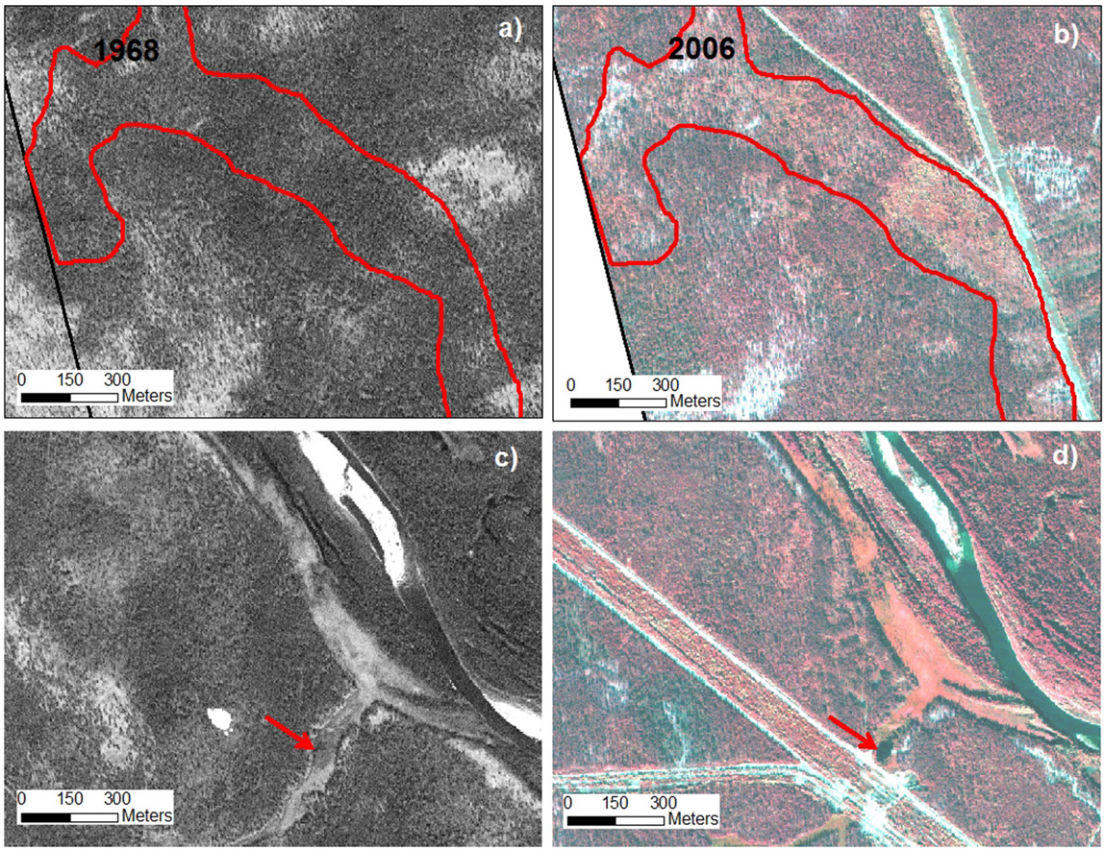

Figure 4. Comparison of land cover types between 1968 Corona and 2006 Quickbird images, showing changes caused by land use. The upper pair shows decreased vegetation cover along the power lines and roads. The lower pair of images indicates accumulation of water (d) in a drained lake basin (c) due to construction of the road resulting in water upstream being channeled into this location.

3.3.3. Spatial patterns caused by disturbance during mid-growing season in multiple years

Mean values of the remotely sensed, land surface indices, focusing on the impacts of disturbance, were assessed and compared during the peak growing season (July–August) for multiple years. Spatially, the NDVI values calculated between 1989 and 2009 were consistently low near disturbances and increased acutely (approximately 0.2 ± 0.02) until approximately 100 m from the disturbance and varied less than ± 0.02 further away from the disturbance (figure 8). The spatial pattern of NDVI on 7/18/2007 is similar to 7/23/2009 in less disturbed areas. The mean NDVI values in disturbed zones (30 and 60 m) on 7/18/2007 are consistently lower than on 7/23/2009 despite almost identical NDVI for distances further from the disturbances. Temporally, the mean NDVI values were consistently lower (approximated 0.2 for NDVI) in years 1989 and 1990 than in the 2000s.

4. Discussion

Multi-temporal and multi-sensor remote sensing data enabled us to assess land cover dynamics in response to climate warming and land use changes. Derived biophysical indices based on multi-spectral imagery also allow quantitative assessment of the spatial patterns of land use change near an oil and gas development site in Northwestern Siberia over the past forty years. Our results document how climate warming and oil and gas development are two major drivers in this region, which transform the landscape with mixed responses of vegetation and hydrological properties.

The high spatial resolution image pair (Corona and Quickbird) allows for the documentation of how the undisturbed areas in the Nadym study region have responded to regional climate change. Mean annual temperature has increased about 2 °C since 1968 in the Nadym region (Vikhamar-Schuler *et al* 2010, Streletskiy *et al* 2012). Such pronounced warming has caused trees (mainly Scots pine (*Pinus sylvestris*) and mountain birch (*Betula tortuosa*) mixed with Siberian larch (*Larix sibirica*)) to expand in portions of the undisturbed regions (figures 3(a) and (b)). This is consistent with the finding in adjacent regions such as Kharp and Obskaya where tall shrub (e.g. alder (*Alnus*)) cover increased by 8.4% and 21% respectively in response to warming (Frost and Epstein 2014). Expansion of boreal trees and shrubs in the Arctic region can result in surface albedo decline during periods of snow cover, and resultant surface energy budget

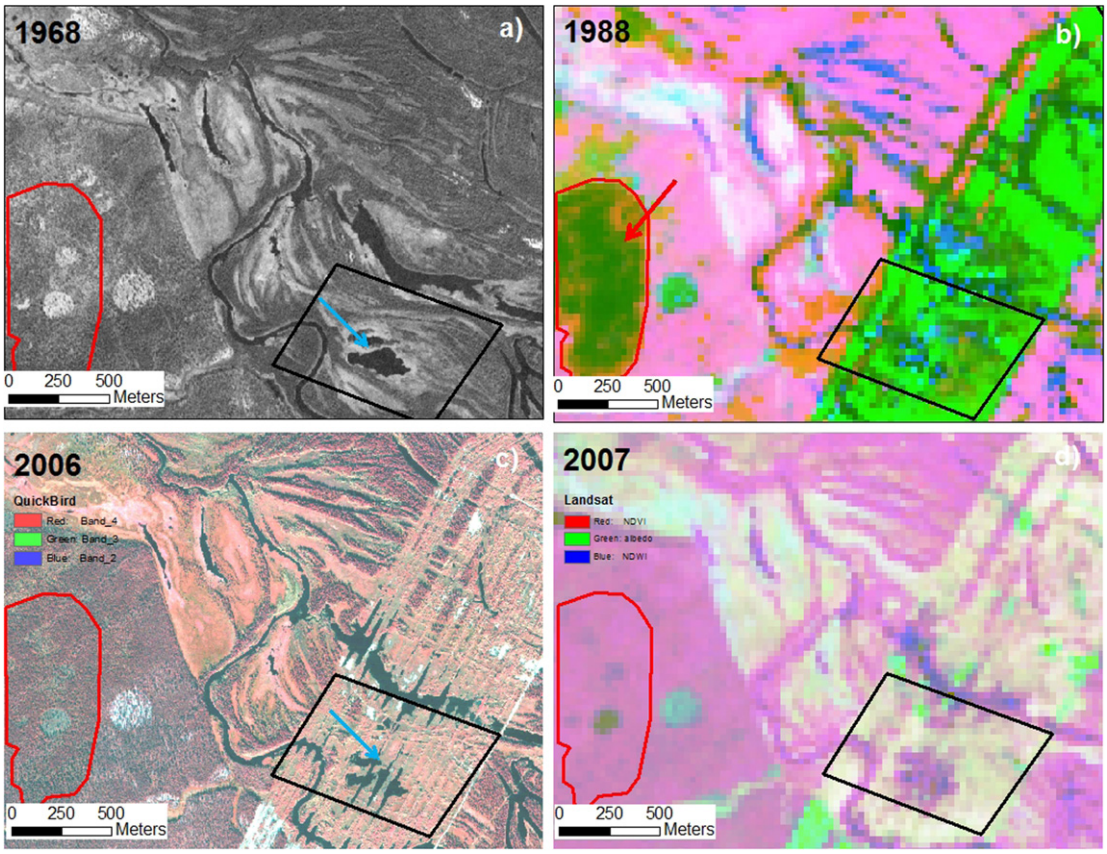

Figure 5. Multi-temporal images show the bidirectional vegetation changes along roads/tracks. Corona (panchromatic) and Quickbird (red-band 4, green-band 3, blue-band 2) images show roads and tracks developed between 1968 and 2006. The blue arrows in the images compare the changes in water bodies from 1968 to 2006 due to the disturbance by vehicle tracks, where thermokarst lakes are being eroded along the disturbance (tracks). Landsat TM images (b), (d) are shown with remote sensing derived-index combinations (red-NDVI, green-albedo, blue-NDWI). The two Landsat-based images show variation in the three biophysical indices. Color red indicates area with abundant vegetation, green indicates low vegetation and high reflective surface and blue indicate high soil moisture. The red arrow points to a disturbed area (likely caused by less severe crown fire), which is low in NDVI and NDWI but not detectable from the VHR pair. The 2007 Landsat scene shows recovery in a majority of that area. The large area in green in the 1988 TM image (b), outlined in black as an example) indicates low NDVI and NDWI compared to other vegetated and water surfaces, suggesting exposed barren ground with disturbed vegetation. In both the 2006 Quickbird image (c) and the 2007 Landsat scene (d), red or pinkish red indicates vegetated surfaces (high NDVI) within the black outline, suggesting a recolonization of vegetation in these previously disturbed areas.

changes when reflective snow cover is replaced with more absorbent vegetation (Loranty *et al* 2011). The increase in tall vegetation can also increase atmospheric heating, as the exposed vegetation absorbs radiation otherwise reflected by snow and reradiates to the surrounding air (Bonan *et al* 1995). Still there are many unknowns about how changes in tall vegetation cover may affect the soil and atmosphere at plot, landscape, and regional scales (Blok *et al* 2010, Lawrence and Swenson 2011). Additionally, decreases in lake sizes were found in undisturbed area (figures 3(c) and (d)). Shrinking and disappearing lakes indicate shifts in drainage pathways and likely are attributed to permafrost degradation in the area (Smith *et al* 2005, Streletskiy *et al* 2012).

The same image pair has also revealed how Nadym region evolved from a natural forest-tundra ecotone to a human modified oil and gas field between 1968 and 2006. A decrease in vegetation cover due to direct impacts from buildings, roads and vehicle tracks, and possibly from forest crown fires associated with the industrial activities is evident (figures 2, 4 and 5). Reduction in tundra vegetation in the Bovanenkovo oil and gas field was also detected using multi-year Landsat and Satellite Pour l'Observation de la Terre scenes (Kumpula *et al* 2012). Negative impacts from oil and gas development in Northwestern Siberia have raised concerns for the ecological environment in these areas (Kumpula *et al* 2011, 2012, Moskalenko 2012). Industrial development has also altered the surface hydrology. A drained-lake basin observed in a 1968 Corona image (e.g. figure 4(c)) accumulated water as the surface hydrology was altered after the construction of a road, and developed into a lake ~50 m wide (figure 4(d)). Waterlogging along the road network may exacerbate permafrost degradation as water absorbs more heat relative to unperturbed vegetation surfaces (Streletskiy *et al* 2014).

Landsat time series provide crucial information for temporal assessments to the high-spatial

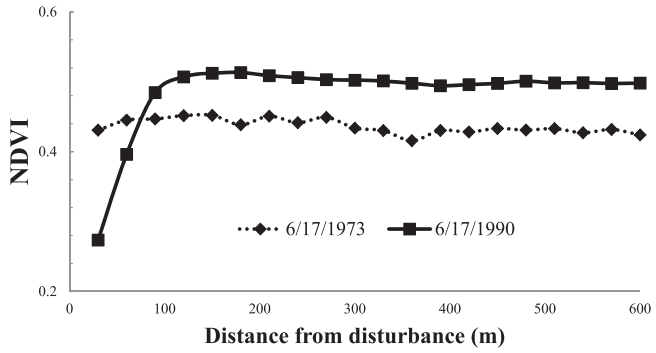

Figure 6. Spatial pattern of mean NDVI based on a buffer zone analysis for 1973 and 1990.

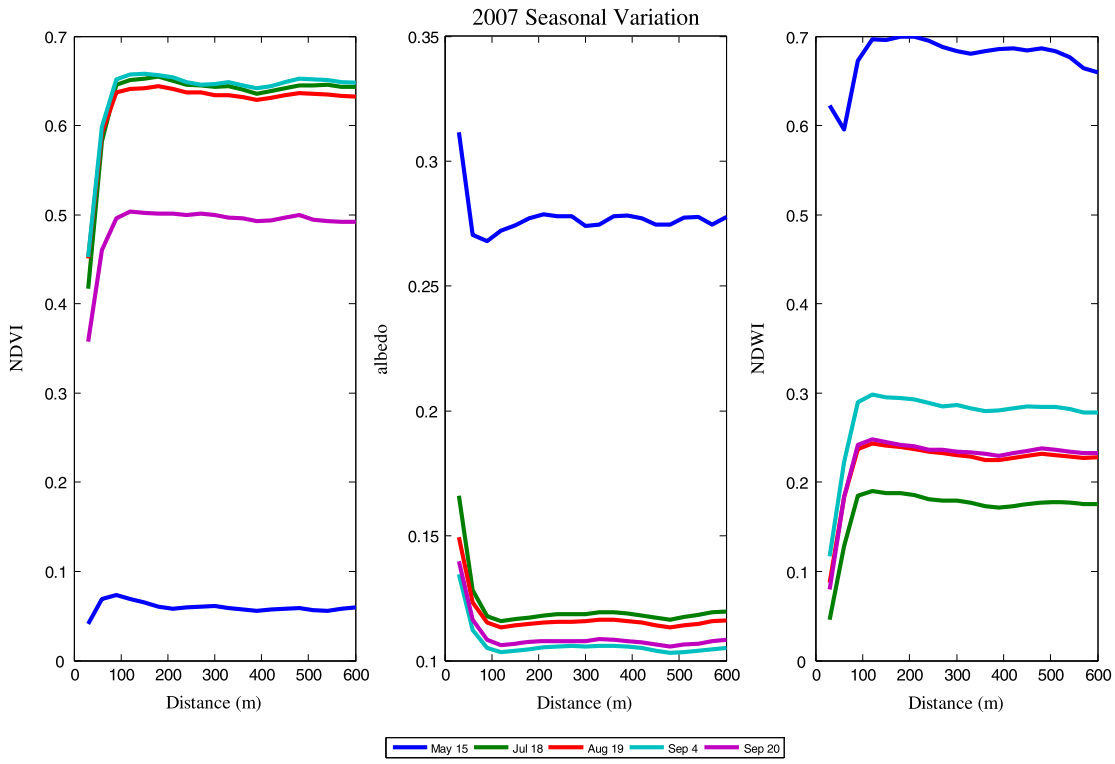

Figure 7. Seasonal changes in NDVI, albedo and NDWI along roads/tracks in year 2007 at distances from roads/tracks up to 600 m.

resolution image pair, which documented end-to-end changes occurring in the study region. Derived biophysical indices facilitate interpretation of changes in the study region (e.g. figure 5, red polygon) although not at the species level. Vegetation decreased in developed areas due to new roads and tracks with declining NDVI, NDWI and increasing albedo in the early 1980s when the development impact was intensive. After establishment of the oil and gas service, the vegetation appears to have started to recover in areas with decreased disturbance intensity. However, the extensive vehicle tracks not only disturb the vegetation cover, but also lead to alteration of the ground thermal regime, thermokarst development, and an increase in erosion rates in locations where they cross lakes and streams (figure 5).

Spatial analysis of Landsat derived indices that assess vegetation productivity, moisture and surface reflectivity reveal that these properties varied significantly within a 100 m distance from the disturbances and then very little beyond that (figure 6). This was supported by analyzing two anniversary Landsat scenes. While the mean NDVI in 1990 was generally greater than in 1973, there is a significant decrease in the first 100 m away from the disturbance that was not present in the earlier image indicating that the vegetation was impacted by the construction and existence of infrastructure (figure 6). In early 1970s, activities associated with oil and gas development had already started but was still likely to be sporadic. Hence, the average NDVI in the 1973 scene does not vary spatially as it does in 1990. Using other

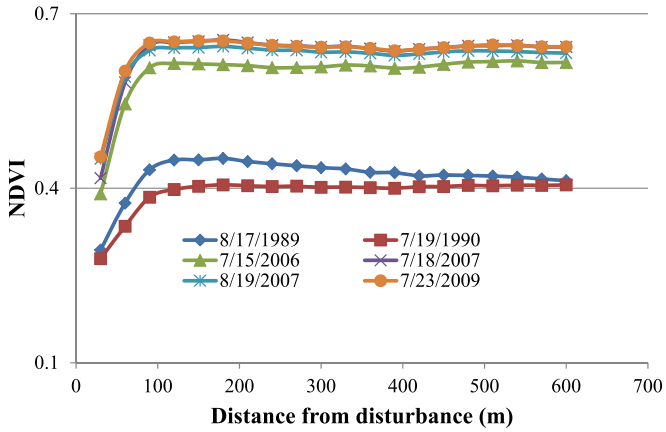

Figure 8. Comparison of image-derived NDVI around roads/tracks along distances up to 600 m. The spatial patterns remain consistent during the 20 year period. In general, NDVI during 2000s is greater than in 1989 and 1990.

available scenes of different years also suggests the existence of spatial patterns due to development (figures 7 and 8). This is similar to what Auerbach *et al* (1997) found in field studies along the Dalton Highway in Alaska where the impact from road dust was pronounced within 100 m of the road (Auerbach *et al* 1997). Image-derived indices also suggest that such effects persist over decades given that the spatial trend away from the developed area did not change substantially over time. Analysis of long-term aerial photographs also confirmed persisting effects of infrastructure in ice-rich permafrost regions in Alaska (Raynolds *et al* 2014). However, we also found some increases in NDVI and decreases in albedo suggesting that vegetation may be recovering along vehicle tracks (figure 5). Growing season NDVI between 1989 and 1990 are generally lower than those in 2000s (figure 8), which may suggest a few ecological processes such as post-disturbance recovery and secondary succession occurred during this period. It can also be attributed to changing climatic conditions in the region where regional climate has warmed (Vikhamar-Schuler *et al* 2010, Streletskiy *et al* 2012, Moskalenko 2013).

Most studies that have focused on the impacts of climate warming on ecosystem and hydrological conditions, this study suggests that industrial development activities can cause substantial changes to ecosystems and hydrological conditions within a 100 m range that may persist over long periods of time. Changes in surface radiation balance associated with vegetation disturbances can lead to permafrost thawing. For example, lowering of the permafrost table to 10 m depth was observed 10 m away from the gas pipeline located in the study area (Ponomareva and Skvortsov 2006). Thawing permafrost can release CH_4 and CO_2 to the atmosphere as anaerobic and aerobic microbial decomposition of previously frozen organic carbon occurs, another positive feedback to the current positive climate anomaly (Christensen *et al* 2004, Schuur *et al* 2008, Tarnocai *et al* 2009, Streletskiy *et al* 2014).

The Nadym region has experienced extensive development both in the city and within the oil and gas development site. Simultaneously, climate warming has caused deeper active layers and permafrost warming (Streleskiy *et al* 2012). Land cover and land use changes due to human activities can interact with climate warming, altering surface energy budgets and having a potentially great impact on arctic systems (Pielke 2002, Hinzman *et al* 2005, Huntington *et al* 2007, Larsen *et al* 2014). The United States Geological Survey has estimated that 30% of the world's undiscovered gas and 13% of the world's undiscovered oil may be found in the Arctic (Gautier *et al* 2009). How oil and gas development may affect arctic terrestrial vegetation, hydrological properties and surface energy budgets is therefore of substantial importance.

5. Conclusion

In this study we investigated the ability to detect land cover change due to climate change and oil/gas development in Northwestern Siberia utilizing multiple sources of remote sensing imagery. High spatial resolution imagery, since the beginning of the satellite era, provided the baseline data that documented the original landscape before heavy anthropogenic land use change began. Modern VHR commercial satellite imagery, when compared with Cold War era Corona imagery, showed changes in the landscape due to climate warming and oil and gas development. Multispectral Landsat series documented the beginning of the construction of oil and gas facilities, the extensive disturbance between 1970s and 1980s, and the partial recovery of vegetation and response to warming in 2000s. Our results suggest that the impacts of development, although spatially confined (within 100 m from disturbed sites), can persist for decades. As oil and gas development is expected to continue, a thorough

understanding of the ecological and environmental consequences is crucial to the sustainability of the fragile arctic environment.

Acknowledgments

This study was supported by NASA/NEESPI Land Cover Land Use Change Initiative, Grant No. NNG6GE00A, NNX09AK56G, and NNX14AD90G. NSF Grant No. ARC-0531180, part of the Synthesis of Arctic System Science initiative, NSF Grant No. ARC-0902152, part of the Changing Seasonality of Arctic Systems initiative, NSF Grant No. OISE-1504221, part of the Promoting Arctic Urban Sustainability in the Arctic, NSF Grant No. PLR-1204110, part of Collaborative Research: Interactions Between Air Temperature, Permafrost and Hydrology in the High Latitudes of Eurasia, and NSF Grant No. ICER1534377, part of Belmont Forum ARCTIC-ERA project by National Research Council of Norway grant 34306/1/ECNS21015N and Russian Science Foundation, project 14-17-00037. Funding from the Department of Environmental Sciences at the University of Virginia made it possible to purchase the high spatial resolution imagery. We thank two anonymous reviewers for constructive comments which helped to improve the quality of the manuscript.

References

ACIA 2005 *Arctic Climate Impact Assessment* (Cambridge: Cambridge University Press) p 1042

Auerbach N A *et al* 1997 Effects of roadside disturbance on substrate and vegetation properties in arctic tundra *Ecol. Appl.* **7** 218–35

Armstrong T, Rogers G and Rowley G 1978 *The Circumpolar North: A Political and Economic Geography of the Arctic and Sub-Arctic* (London: Methuen)

Bhatt U S *et al* 2010 Circumpolar arctic tundra vegetation change is linked to sea ice decline *Earth Interact.* **14** 1–20

Bhatt U S, Walker D A, Raynolds M K, Bieniek P A, Epstein H E, Comiso J C, Pinzon J E, Tucker C J and Polyakov I V 2013 Recent declines in warming and vegetation greening trends over pan-Arctic tundra *Remote Sens.* **5** 4229–54

Blok D, Heijmans M M P D, Schaepman-Strub G, Kononov A V, Maximov T C and Berendse F 2010 Shrub expansion may reduce summer permafrost thaw in Siberian tundra *Glob. Change Biol.* **16** 1296–305

Bonan G B, Chapin F S and Thompson S L 1995 Boreal forest and tundra ecosystems as components of the climate system *Clim. Change* **29** 145–67

Carlson T N and Ripley D A 1997 On the relation between NDVI, fractional vegetation cover, and leaf area index *Remote Sens. Environ.* **62** 241–52

Chapin F S III *et al* 2005 Role of land-surface changes in arctic summer warming *Science* **310** 657–60

Christensen T R, Johansson T, Akerman H J, Mastepanov M, Malmer N, Friborg T, Crill P and Svensson B H 2004 Thawing sub-arctic permafrost: effects on vegetation and methane emissions *Geophys. Res. Lett.* **31** L04501

Epstein H E, Raynolds M K, Walker D A, Bhatt U S, Tucker C J and Pinzon J E 2012 Dynamics of aboveground phytomass of the circumpolar Arctic tundra during the past three decades *Environ. Res. Lett.* **7** 015506

Flanders N E, Brown R V, Andre'eva Y and Larichev O 1998 Justifying public decisions in Arctic oil and gas development: American and Russian approaches *Arctic* **51** 262–79

Forbes B *et al* 2001 Anthropogenic disturbance and patch dynamics in circumpolar arctic ecosystems *Conservation Biol.* **15** 954–69

Forbes B, Boelter M, Mueller-Wille L, Hukkinen J, Mueller F, Gunslay N and Konstantinov Y 2006 *Reindeer Management in Northernmost Europe* (Berlin: Springer)

Forbes B C, Stammler F, Kumpula T, Meschtyb N, Pajunen A and Kaarlejaervi E 2009 High resilience in the Yamal-Nenets social-ecological system, West Siberian Arctic, Russia *Proc. Natl Acad. Sci. USA* **106** 22041

Ford J D *et al* 2006 Vulnerability to climate change in the Arctic: a case study from Arctic Bay, Canada *Glob. Environ. Change* **16** 145–60

Frost G V and Epstein H E 2014 Tall shrub and tree expansion in Siberian tundra ecotones since the 1960s *Glob. Change Biol.* **20** 1264–77

Frost G V, Epstein H E, Walker D A, Matyshak G and Ermokhina K 2013 Patterned-ground facilitates shrub expansion in Low Arctic tundra *Environ. Res. Lett.* **8** 015035

Gao B 1996 NDWI—a normalized difference water index for remote sensing of vegetation liquid water from space *Remote Sens. Environ.* **58** 257–66

Gautier D L, Bird K J, Charpentier R R, Grantz A, Houseknecht D W, Klett T R, Moore T E, Pitman J K, Schenk C J and Schuenemeyer J H 2009 Assessment of undiscovered oil and gas in the Arctic *Science* **324** 1175–9

Goetz S J *et al* 2005 Satellite-observed photosynthetic trends across boreal North America associated with climate and fire disturbance *Proc. Natl Acad. Sci. USA* **102** 13521

Grosse G, Schirrmeister L, Kunitsky V V and Hubberten H-W 2005 The use of CORONA images in remote sensing of periglacial geomorphology: an illustration from the NE Siberian coast *Permafrost Periglacial Process.* **16** 163–72

Hinzman L D *et al* 2005 Evidence and implications of recent climate change in Northern Alaska and other arctic regions *Clim. Change* **72** 251–98

Huntington H *et al* 2007 The influence of human activity in the Arctic on climate and climate impacts *Clim. Change* **82** 77–92

Jia G J *et al* 2003 Greening of arctic Alaska, 1981–2001 *Geophys. Res. Lett.* **30** 2067

Khitun O, Rebristaya O, Watson A E and Alessa L 2001 *Anthropogenic Impacts on Habitat Structure and Species Richness in the West Siberian Arctic* USDA Forest Service Rocky Mountain Research Station, 2150 Centre Avenue Fort Collins CO 80526 USA

Kumpula T, Forbes B C and Stammler F 2010 Remote sensing and local knowledge of hydrocarbon exploitation: the case of Bovanenkovo, Yamal Peninsula, West Siberia, Russia *Arctic* **63** 165–78

Kumpula T, Forbes B C, Stammler F and Meschtyb N 2012 Dynamics of a coupled system: multi-resolution remote sensing in assessing social-ecological responses during 25 years of gas field development in Arctic Russia *Remote Sensing* **4** 1046–68

Kumpula T *et al* 2011 Land use and land cover change in Arctic Russia: ecological and social implications of industrial development *Glob. Environ. Change* **21** 550–62

Lawrence D M and Swenson S C 2011 Permafrost response to increasing Arctic shrub abundance depends on the relative influence of shrubs on local soil cooling versus large-scale climate warming *Environ. Res. Lett.* **6** 045504

Larsen J N, Anisimov O A, Constable A, Hollowed A B, Maynard N, Prestrud P, Prowse T D and Stone J M R 2014 Polar regions *Climate Change 2014: Impacts, Adaptation, and Vulnerability, Part B: Regional Aspects, Contribution of Working Group II to the Fifth Assessment Report of the Intergovernmental Panel of Climate Change* ed V R Barros *et al* (Cambridge: Cambridge University Press) pp 1567–612

Larsen J N and Fondahl G 2015 *Arctic Human Development Report: Regional Processes and Global Linkages* Nordic Council of Ministers

Liang S 2001 Narrowband to broadband conversions of land surface albedo I-Algorithms *Remote Sens. Environ.* **76** 213–38
Loranty M M, Goetz S and Beck P S A 2011 Tundra vegetation effects on pan-Arctic albedo *Environ. Res. Lett.* **6** 024014
Masek J *et al* 2006 A Landsat surface reflectance dataset for North America, 1990–2000 *IEEE Geosci. Remote Sens. Lett.* **3** 68–72
Moskalenko N 2003 Interactions between vegetation and permafrost on some CALM grids in Russia *Permafrost: Proc. 8th Int. Conf. on Permafrost* (Zurich, Switzerland: AA Balkema Publishers) pp 789–94
Moskalenko N, Lewkowicz A and Allard M 1998 Impact of vegetation removal and its recovery after disturbance on permafrost *Proc. 7th Int. Conf. on Permafrost* pp 763–70
Moskalenko N G 2012a Cryogenic landscape changes in the West Siberia Northern taiga in climate change conditions and human-induced disturbances *Earth Cryosphere* **XVI** 38–42
Moskalenko N G 2012b Impact of permafrost degradation on Northern Taiga ecosystems in Western Siberia *Proc. 10th Int. Conf. on Permafrost* (*Salekhard, 2012*) vol 2 pp 281–6
Moskalenko N G 2013 Impact of climate warming on vegetation cover and permafrost in West Siberia northern Taiga *Nat. Sci.* **5** 144–8
Perovich D, Gerland S, Hendricks S, Meier W, Nicolaus M, Richter-Menge J and Tschudi M 2013 Sea Ice *Arctic Report Card 2013*
Pielke R A 2002 The influence of land-use change and landscape dynamics on the climate system: relevance to climate-change policy beyond the radiative effect of greenhouse gases *Phil. Trans. R. Soc.* A **360** 1705–19
Ponomareva O E and Skvortsov A G 2006 Methods and results of studying of exogeneous geological processes in Nadym area of Western Siberia *The Theory and Practice of an Estimation of the Earth Cryosphere State and the Forecast of its Change: Materials of Int. Conf.* (*Tyumen, GNGU*) vol 1 pp 272–4
Raynolds M K, Walker D A, Ambrosius K J, Brown J, Everett K R, Kanevskiy M, Kofinas G P, Romanovsky V E, Shur Y and Webber P J 2014 Cumulative geoecological effects of 62 years of infrastructure and climate change in ice-rich permafrost landscapes, Prudhoe Bay Oilfield, Alaska *Glob. Change Biol.* **20** 1211–24
Rouse J *et al* 1974 Monitoring the vernal advancement and retrogradation (green wave effect) of natural vegetation *NASA/GSFC Type III Final Report* Greenbelt, Md p 371
Schuur E A G *et al* 2008 Vulnerability of permafrost carbon to climate change: implications for the global carbon cycle *BioScience* **58** 701–14
Smith L *et al* 2005 Disappearing arctic lakes *Science* **308** 1429
Streletskiy D A, Anisimov O A and Vasiliev A A 2014 Permafrost degradation *Snow and Ice-Related Risks, Hazards and Disasters* ed W Haeberli and C Whiteman (Oxford: Elsevier) pp 303–44
Streletskiy D A, Shiklomanov N I and Grebenets V I 2012 Changes of foundation bearing capacity due to climate warming in Northwest Siberia *Earth Cryosphere* **XVI** 22–32 (in Russian)
Stroeve J C, Serreze M C, Holland M M, Kay J E, Malanik J and Barrett A P 2012 The Arctic's rapidly shrinking sea ice cover: a research synthesis *Clim. Change* **110** 1005–27
Tarnocai C, Canadell J G, Schuur E A G, Kuhry P, Mazhitova G and Zimov S 2009 Soil organic carbon pools in the Northern circumpolar permafrost region *Glob. Biogeochem. Cycles* **23** GB2023
Turner B *et al* 2003 Illustrating the coupled human-environment system for vulnerability analysis: three case studies *Proc. Natl Acad. Sci.* **100** 8080–5
Turner B, Skole D, Sanderson S, Fischer G, Fresco L and Leemans R 1995 *Land-Use and Land-Cover Change: Science/Research Plan* Report No. 35/7 (Stockholm: Royal Swedish Academy of Sciences)
Vasiliev A, Drozdov D and Moskalenko N 2008a Dynamics of permafrost temperature in West Siberia under changing climate *Earth Cryosphere* **XII** 10–8
Vasiliev A, Leibman M and Moskalenko N 2008b Active layer monitoring in West Siberia under the CALM II Program *Proc. 9th Int. Conf. on Permafrost* (*Institute of Northern Engineering, University of Alaska, Fairbanks*) vol 2 pp 1815–1821
Vikhamar-Schuler D, Inger H-B and Eirik J F 2010 *Long-Term Climate Trends of the Yamalo-Nenets AO, Russia.* met. no report
Walker D A and Walker M D 1991 History and pattern of disturbance in Alaskan Arctic Terrestrial Ecosystems: a hierarchical approach to analysing landscape change *J. Appl. Ecol.* **28** 244–76
Walker D A *et al* 1987 Cumulative impacts of oil fields on Northern Alaskan Landscapes *Science* **238** 757–61
Walker D A, Epstein H E, Leibman M E, Moskalenko N G, Kuss J P, Matyshak G V, Kaärlejarvi E, Forbes B C and Barbour E M 2008 Data report of the 2007 expedition to Nadym, Laborovaya and Vaskiny Dachi, Yamal Peninsula Region, Russia
Walker D A *et al* 2009 Spatial and temporal patterns of greenness on the Yamal Peninsula, Russia: interactions of ecological and social factors affecting Arctic NDVI *Environ. Res. Lett.* **4** 045004
Walker D A, Forbes B C, Leibman M O, Epstein H E, Bhatt U S, Comiso J C, Drozdov D S, Gubarkov A A, Jia G J and Kaarlejärvi E 2011 Cumulative effects of rapid land-cover and land-use changes on the Yamal Peninsula, Russia *Eurasian Arctic Land Cover and Land Use in a Changing Climate* (Berlin: Springer) pp 207–36